

THE DYNAMICS OF THE VORTICITY FIELD IN A LOW SOLIDITY AXIAL TURBINE

K. G. Barmpalias, A. I. Kalfas¹, N. Chokani, R. S. Abhari

LSM, Turbomachinery Laboratory
 Department of Mechanical and Process Engineering
 ETH Zurich
 Zurich, Switzerland

ABSTRACT

A current trend in turbomachinery design is the use of low solidity axial turbines that can generate a given power with fewer blades. However, due to the higher turning of the flow, relative to a high solidity turbine, there is an increase in secondary flows and their associated losses. In order to increase the efficiency of these more highly loaded stages, an improved understanding of the mechanisms related to the development, evolution and unsteady interaction of the secondary flows is required. An experimental investigation of the unsteady vorticity field in highly loaded stages of a research turbine is presented here. The research turbine facility is equipped with a two-stage axial turbine that is representative of the high-pressure section of a steam turbine. Steady and unsteady area measurements are performed, with the use of miniature pneumatic and fast response aerodynamic probes, in closely spaced planes at the exits of each blade row. In addition to the 3D total pressure flowfield, the multi-plane measurements allow the full three-dimensional time-resolved vorticity and velocity fields to be determined. These measurements are then used to describe the development, evolution and unsteady interaction of the secondary flows and loss generation. Particular emphasis is given to the vortex stretching term of the vorticity transport equation, which gives new insight into the vortex tilting and stretching that is associated with the secondary loss generation.

INTRODUCTION

Low solidity blade design is beneficial in terms of low production cost and reduced machining time. However the use of fewer blades leads to thicker wakes and increased secondary losses.

¹Current address: Aristotle University of Thessaloniki, Greece

Significant effort has been devoted the to understanding of unsteady flow interactions. In the reviews of Langston (2001) and Sieverding (1985) concerning secondary flows the major source of loss is identified as the viscous dissipative forces as they arise between the secondary flow and the blade's suction side. In 1997, Halstead et al. presented a comprehensive study of the boundary layer development in compressors and turbines of multistage machines. The effects of the loading variation and nozzle-nozzle interaction were discussed in part 1 of the paper, which provides a composite picture. These observations are particularly interesting in the strive for a lighter blading arrangement involving low solidity vanes. In the recent literature, a number of studies have dealt with the kinematics of wake convection through turbine blading. Stieger and Hodson (2005) have shown experimentally the mechanisms of turbulent kinetic energy production in the boundary layers of low pressure turbines, using laser velocimetry. These studies focus primarily on low pressure turbines with high aspect ratio blading that operate in Reynolds number ranges where transition may affect significantly the boundary layer development. In an early study, Sharma et al. (1985) have shown various effects of 3D unsteady flow in axial flow turbines. In their study they used fast response velocimetry to identify the various potential flow field effects as well as viscous flow regions. In low aspect ratio machines, many investigators found, in addition to the well established hub and tip passages vortices, other vortical structures, (e.g., Binder and Romey (1983) and Zaccaria and Lakshiminarayama (1985)). In a more recent study Pullan et al. (2002) presented an experimental and computational study of the formation of a streamwise shed vortex in a low aspect ratio turbine stage. The effect of the perturbation from the blade trailing shape on the wake shear layer was shown to be the tendency of the wake to roll up into a streamwise vortex. Furthermore, Miller et al. (2003) showed the effects of an interstage swan-

necked diffuser on the vorticity field in the exit flow of a relatively low aspect ratio turbine. In his work on the loss mechanisms in turbomachines, Denton (1993) suggested that the swirl velocity between main and leakage flow dominates the mixing losses. Schlienger et al. (2004) investigated the use of inserts in the inlet cavities as a means to control secondary flows. Tsuguhisa et al. (2007) examined the blade loading influence in axial steam turbine stator blades with respect to efficiency and found that although fewer blade count produced wider wakes and vortices, there was a benefit in the overall performance. Chaluvadi et al. (2003) studied the impact of the upstream rotor passage on the downstream stator blade row. Treiber et al. (2002) used detailed pneumatic probe measurements to show the effect of blade geometry on the evolution of the secondary flow. Rusch et al. (2004) evaluated the vorticity stretching term of the unsteady vorticity transport equation to describe the inlet cavity of an axial turbine.

This paper focuses on the development, evolution and unsteady interaction of secondary flows. This is accomplished from multi-plane measurements downstream of a stator row in an axial research turbine. The closely spaced multi-plane measurements allow the full three-dimensional time-resolved total pressure, vorticity and velocity fields to be determined. The vortex stretching and tilting terms of the unsteady vorticity transport equation are evaluated and related to the secondary loss generation mechanisms. It is shown that the terms have different influences on the transport of loss generation. This improved knowledge offers a turbine designer instructive guidelines to achieve enhanced performance.

NOMENCLATURE

AR	aspect ratio
C	chord length
C_{ax}	axial chord
C_p	stagnation pressure coefficient
	$(P_{t,i} - P_{t,i=3}) / \left(0.5 \cdot \bar{\rho}_3 \cdot (\bar{v}_z / \cos 70^\circ)^2 \right)$
C_{pt}	pressure coefficient
	$(P_t - P_{s,exit}) / (P_{t,inlet} - P_{s,exit})$
ΔC_{pt}	$(C_{pt,max} - C_{pt})$
H	blade span
M	Mach number
ns	streamwise normal direction
P	pressure
s	streamwise direction
t	time
T	stator pitch
t/T_o	fraction of blade passing period
T_o	blade passing period
x, y, z	Cartesian coordinates
Δx	distance downstream of LS stator
z	axial direction
<i>Greek</i>	
α	absolute flow yaw angle
γ	pitch

σ	solidity
ϕ	flow coefficient
ρ	density
ψ	stage loading coefficient
ω	vorticity
V	velocity

Abbreviations

5HP	five hole probe
FRAP	Fast Response Aerodynamic Probe
HS, LS	high solidity stator, low solidity stator
PS, SS	pressure side, suction side
TE, LE	trailing edge, leading edge

Subscripts

ns	streamwise normal direction
s	streamwise direction, static condition
R	rotor
S	stator
t	total condition

Superscripts

\rightarrow	vector
---------------	--------

EXPERIMENTAL METHOD

The research facility

The measurements were performed in the two stage axial research turbine 'LISA' at the Turbomachinery Laboratory of the ETH Zurich. The turbine inlet temperature TET is kept constant at 310 K with an accuracy of 0.9 K. A DC generator maintains a constant operating speed of 2750 \pm 0.5 RPM (\pm 0.02%). A more detailed description of the test facility is available in Schlienger et al. (2004). The stator blade row configurations are different as shown in Table 1. The upstream stator is of a high solidity (1.43) design whereas the downstream stator has a low solidity (1.25). Both stators are designed to have the same exit flow angle and axial chord. The associated operating parameters based on the LS stator are summarized in Table 2.

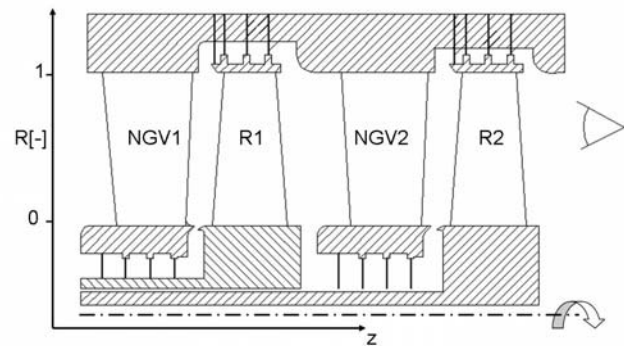


Figure 1: Schematic diagram of the two stage axial turbine

Parameter	HS stator	LS stator
Blade count Z_s	48	36
Axial chord* C_{ax} [mm]	50	50
Chord length* C [mm]	66.3	77.4
Pitch* T [mm]	46.5	62.0
Blade height H [mm]	90	90
Aspect ratio $AR = H/C$ [-]	1.36	1.16
Solidity $\sigma = C/T$ [-]	1.43	1.25

Table 1: Geometric details of stator blades.
(* indicates that dimension is at 50% span)

Rotor speed [RPM]	2750
Overall pressure ratio [-]	1.32
Mass flow [kg/sec]	7.87
Turbine inlet temperature [°C]	37.8
Blade number count stage-1 (stator/rotor)	48/48
Blade number count stage-2 (stator/rotor)	36/48
Tip/hub diameter [mm]	800/620
Flow coefficient (stage-2) [-]	0.3
Loading coefficient (stage-2) [-]	1.0
Mach number (stator/rotor)	0.32/0.1
Reynolds number (rotor)	2×10^5

Table 2. Main parameters of the test case configuration based on the LS stator's characteristics

Instrumentation

Both steady and unsteady flowfield measurements are made. The steady flow field is measured with a 5-hole probe having a 0.9 mm head diameter, whereas the unsteady flowfield is captured with the use of 2-sensor Fast Response Aerodynamic Probe (FRAP), which has a 1.8 mm head diameter, Fig. 2. The FRAP has a measurement bandwidth of 40 kHz. The measured flow parameters and their absolute uncertainties are listed in Table 3. The use of these probes in the turbine facility 'LISA' has been shown in several publications, including Lenherr et al. (2007).

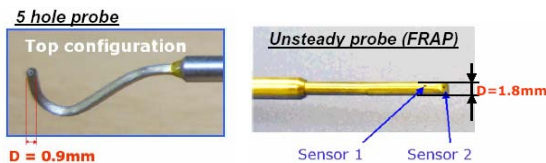


Figure 2: 5HP and FRAP measurement probes

	α	γ	P_t	P_s	M
FRAP	0.3°	0.3°	100 Pa	150 Pa	0.5%
5HP	0.3°	0.3°	60 Pa	150 Pa	0.4%

Table 3: Uncertainties in probe measurements

Probe measurements were made at the rotor exits and downstream of the LS stator. Downstream of the stator, measurements are made in five planes equally spaced by 0.5 mm. At mid-span, the blade row spacing between the LS stator and second rotor is $0.358C_{ax}$, and the first and last

planes are $0.17C_{ax}$ and $0.21C_{ax}$ downstream of the stator trailing edge. The measurement grids consist of 46 points and 61 points evenly distributed in the radial and circumferential directions respectively. The circumferential traverse was conducted over three LS stator pitches. Data are sampled at 200 kHz, which corresponds to 92 samples per blade-passing period. A phase-lock data averaging procedure is performed over 88 rotor revolutions.

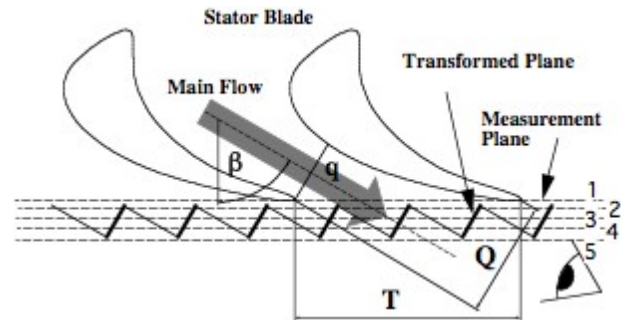


Figure 3: Illustration of the rotation measurement plane, in (x, y, z) axes, to a view in a transformed plane, (sn, y, s) axes

STRETCHING AND TILTING OF VORTICITY

The three components of the vorticity vector

$$\vec{\omega} = \nabla \times \vec{v} \quad (1)$$

can be written as

$$\begin{aligned} \omega_x &= \frac{\partial v_z}{\partial y} - \frac{\partial v_y}{\partial z} \\ \omega_y &= \frac{\partial v_x}{\partial z} - \frac{\partial v_z}{\partial x} \\ \omega_z &= \frac{\partial v_y}{\partial x} - \frac{\partial v_x}{\partial y} \end{aligned} \quad (2)$$

In previous studies concerning the development of streamwise vorticity, the tangential (or streamwise normal) and radial components are approximated, since the spatial resolution of the axial (or streamwise) measurement planes is poor. Gregory-Smith et al. (1987) proposed the use of an incompressible Helmholtz equation as an aid to estimate the tangential and radial vorticity components from the measured axial vorticity component. No such approximation is necessary in the present work as the 3D spatial resolution of the measurement grid is sufficiently fine. Thus from the three-dimensional, time-resolved vorticity and velocity fields, the evaluation of the first term of the unsteady vorticity transport equation

$$\frac{D}{Dt} \left(\frac{\vec{\omega}}{\rho} \right) = \frac{1}{\rho} \vec{\omega} \cdot \nabla \vec{v} + \frac{1}{\rho^3} \nabla \rho \times \nabla p + \frac{1}{\rho^2} \nabla \times \nabla \cdot \tau + \frac{1}{\rho} \left(\nabla \frac{1}{\rho} \right) \times \nabla \cdot \tau \quad (3)$$

is straight forward. This term, the product of vorticity and the rate of change of velocity with respect to the distance along the vortex line, describes the vortex tilting and stretching, Greitzer et al. (2004). The second term in Eq. (3), the baroclinic generation is directly related to the entropy distribution and requires time resolved temperature measurements to be evaluated. The third term requires stress measurements to be evaluated; the second and third terms are not considered in the present work. In matrix form the first term of Eq. (3) can be rewritten as

$$\frac{1}{\rho} \begin{bmatrix} \vec{\omega} \cdot \nabla \vec{v} \\ \vec{\omega} \cdot \nabla \vec{v} \\ \vec{\omega} \cdot \nabla \vec{v} \end{bmatrix} = \frac{1}{\rho} \begin{bmatrix} \omega_x \frac{\partial v_x}{\partial x} + \omega_y \frac{\partial v_x}{\partial y} + \omega_z \frac{\partial v_x}{\partial z} \\ \omega_x \frac{\partial v_y}{\partial x} + \omega_y \frac{\partial v_y}{\partial y} + \omega_z \frac{\partial v_y}{\partial z} \\ \omega_x \frac{\partial v_z}{\partial x} + \omega_y \frac{\partial v_z}{\partial y} + \omega_z \frac{\partial v_z}{\partial z} \end{bmatrix} \quad (4)$$

Instead of the more conventional x, y, z axes, the multiplane measurements can be viewed from rotated axes that are oriented along the streamwise normal (sn), radial (y), and streamwise (s), directions. This perspective provides a clearer view of the evolution of the wake and vortices relative to the passage throat, as shown in Fig. 3. In the sn, y, s axes system, the corresponding nine terms of the matrix, Eq. (4), can be illustrated as shown in Fig. 4. It can be seen that the main diagonal is composed of the vortex stretching-squeezing elements in which the velocity gradient is in the same direction as the vorticity component. The other six elements of the matrix represent the vortex tilting terms.

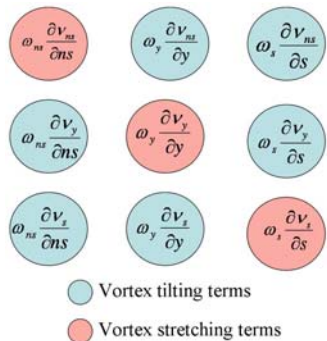


Figure 4: Representation of vortex stretching and tilting terms of the matrix Eq. (4) in (sn, y, s) axes

In Fig. 5, the stretching-tilting mechanism is graphically illustrated for the third row of terms in Fig. 4, in order to aid the interpretation of the results presented below.

The velocity field is assumed to have positive velocity gradient components. In the streamwise direction as the velocity gradient is aligned with the streamwise vorticity, the effect is that the vorticity is stretched as flow evolves downstream. In the sn and y directions, the velocity gradients and vorticity components are orthogonal; thus as the flow evolves the vorticity components are tilted. The no-slip boundary condition on the blade, hub and casing surfaces are the source of vorticity generation. The stretching and tilting of this vorticity as it is transported by wakes and secondary flow, is also accompanied by dissipation that leads to loss generation.

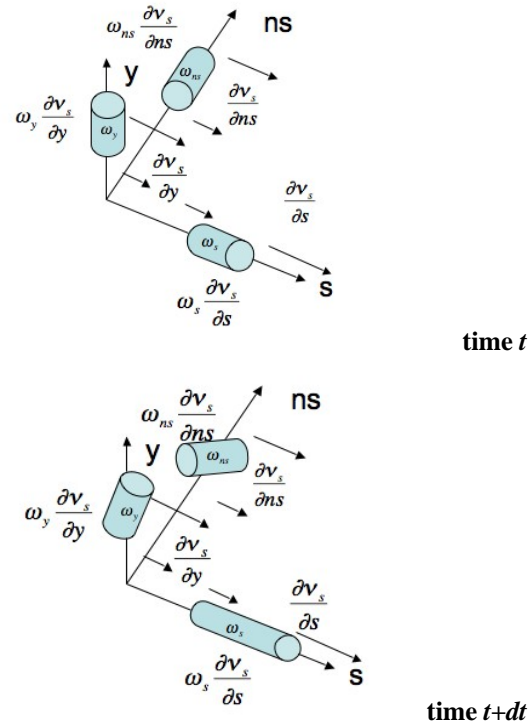


Figure 5: Illustration of stretching-tilting of vorticity components, initially, at time t , and later, at time $t+dt$

RESULTS AND DISCUSSION

In Fig. 6, the nine elements of the vortex stretching-tilting matrix, Fig. 4, are shown time averaged for the most downstream LS stator measurement plane. The stator wakes are clearly identifiable in all nine terms. In terms of the vortex stretching, the streamwise and streamwise normal terms are the most significant terms. The streamwise squeezing of the wake is most dominant in the second and third stator passages, whereas in the first passage the wake's streamwise squeezing is confined to the upper half of the passage and streamwise stretching occurs in the lower half. The different blade counts between the two stators contributes to non-uniformity in the flow field. The streamwise normal is less dominant, and shows that stretching of the wake in the streamwise normal direction

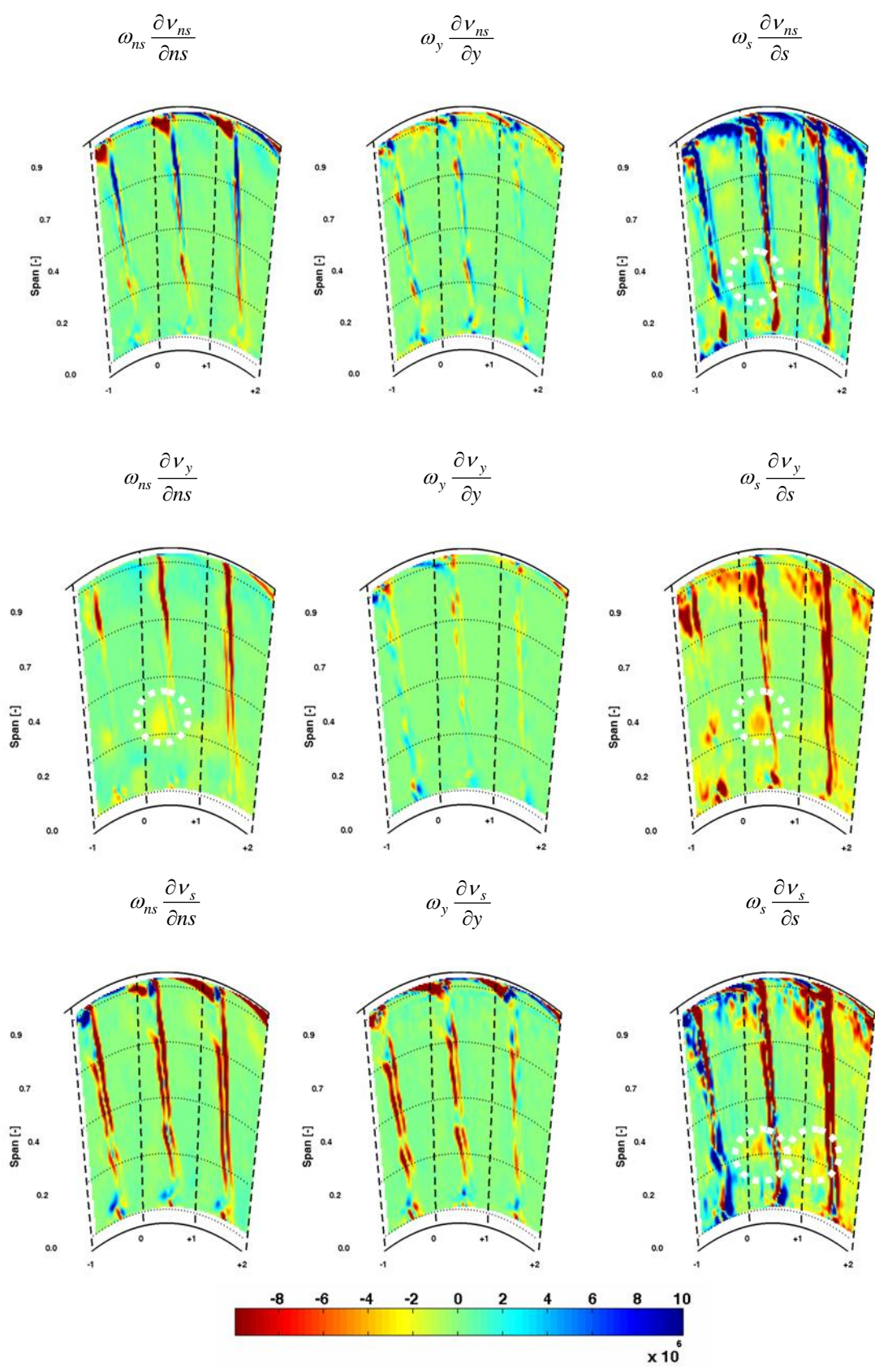


Figure 6: Time averaged vortex stretching–tilting at exit of LS stator. Most downstream measurement plane.

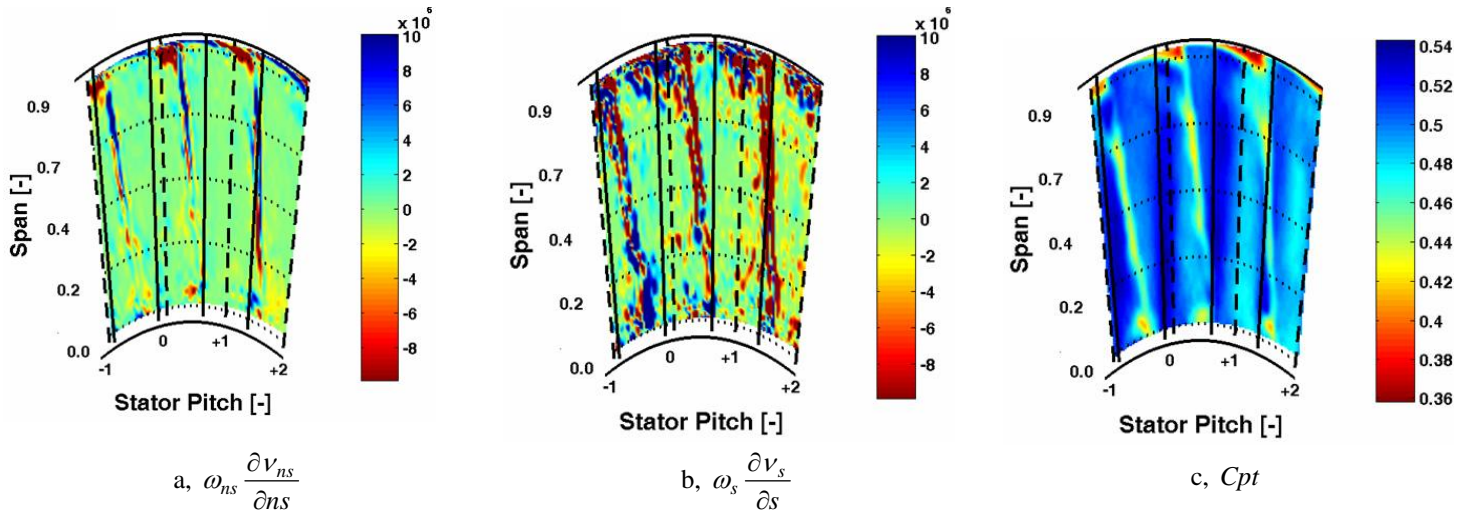


Figure 7: Time resolved flow field at most downstream measurement plane of LS stator exit, $t/T_o = 0.02$. a) streamwise normal vorticity stretching term; b) streamwise vorticity stretching term; and c) stagnation pressure coefficient

occurs over the stator blade pressure sides in the upper half of the passages and streamwise normal squeezing in the lower halves of the passages on the stator blade suction sides. In all three passages strong streamwise squeezing is seen to occur at $Span = 0.20$; these are remnants of non-indigenous secondary flow features shown as the region with white dotted circles, Fig.6 that originate in the HS stator and are convected downstream, being chopped by the first rotor blades as they evolve. The streamwise normal squeezing of the indigenous tip vortices is also quite evident, and will be discussed in detail below. Although the wake is the dominant flow feature, the stretching/squeezing of the radial vorticity is considerably smaller since the radial gradient of the radial velocity is negligible, despite the fact that the radial vorticity is large. The

tendency of the shear layers, which are shed from the stator's pressure and suction sides, to deviate towards the suction side can be seen from the tilting term $\omega_{ns}(\partial v_s / \partial ns)$ that is negative along the span of the wake. In the time resolved flowfields that are presented below, the interaction between the casing new boundary layer and the tip vortex is discussed. On account of the different blade counts in stator and rotor blade rows, in the second and third passages, the tip vortices are deviated in the same direction as the wake. However, the tip vortex from the first passage is deviated in the opposite direction due to the close proximity of downstream rotor's suction side

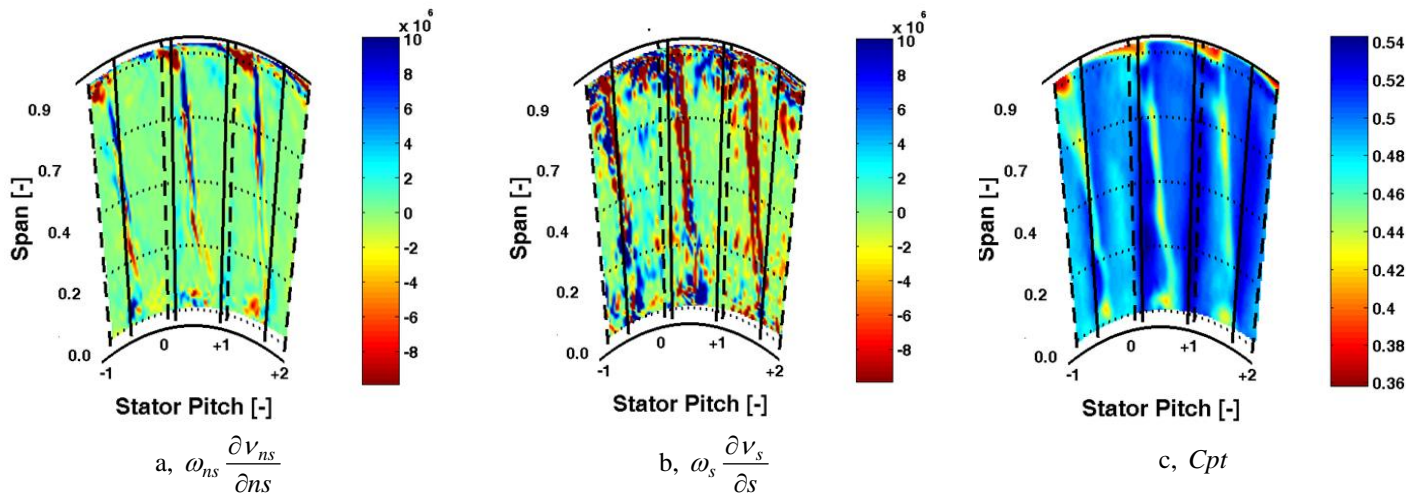


Figure 8: Time resolved flow field at most downstream measurement plane of LS stator exit, $t/T_o = 0.12$. a) streamwise normal vorticity stretching term; b) streamwise vorticity stretching term; and c) stagnation pressure coefficient

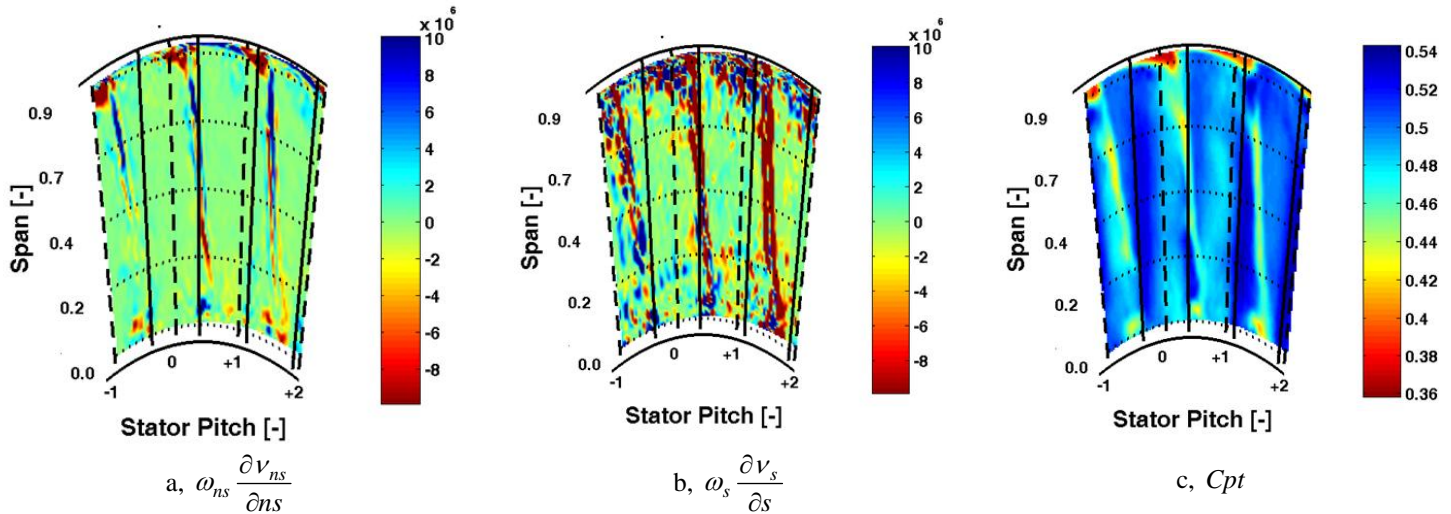


Figure 9: Time resolved flow field at most downstream measurement plane of LS stator exit, $t/T_o = 0.20$. a) streamwise normal vorticity stretching term; b) streamwise vorticity stretching term; and c) stagnation pressure coefficient

Time Resolved Flow Field

The time-resolved flow field is next examined at $t/T_o=0.02, 0.12$ and 0.20 . The location of the rotor blade leading edge's are shown as solid black lines. Over a time increment of $\Delta t/T_o=0.08$, a rotor blade travels over one third of a rotor pitch. At $t/T_o=0.02$, the downstream rotor blade at $Stator\ Pitch = -1$ intersects the tip passage vortex, whereas the tip passage vortices originating from the adjacent stator blades are convected through rotor passages. Therefore at each time $t/T_o=0.02, 0.12$ and 0.20 , a rotor blade is intersecting a tip passage vortex. In Figs. 7-9, the flow fields of the streamwise and streamwise normal vorticity stretching terms are presented together with the corresponding stagnation pressure coefficients. Positive values of the stretching terms indicate an elongation of a flow feature, whereas negative values are associated with its compression. In Fig. 7, it can be seen that the tip passage vortices which are convected through the rotor passages have the largest streamwise normal compression, whereas the compression of the vortex that intersects the rotor is less. Both vortices that are convected through the rotor passages interact with the casing boundary layer that is just downstream of the stator trailing edge. This skewed boundary layer originates as the new boundary layer that is left behind by the passage vortex. Within the rotor passage, this skewed boundary layer tends to move from one stator blade pressure side to another blade's suction side. As the boundary layer leaves the passage, at the stator blade's trailing edge, it tends to move from the suction side to the pressure side in the streamwise normal direction. On the otherhand, on the pressure side of the stator blade's trailing edge, the wake is the dominant flow feature in the tip region. The negative radial vorticity of the wake moves fluid towards the suction side. As the tip vortex is in between these two opposite motions, it is squeezed in the streamwise normal direction and thus elongated in the streamwise direction. It is this mechanism –

vortex squeezing in the streamwise normal direction and vortex elongation in the streamwise direction – that leads to the higher losses in the passage vortices that are seen in Fig. 7c. It is also significant to note that the tip passage vortex at $Stator\ Pitch = 1$, has higher losses, since at this time $t/T_o=0.02$, the rotor blade that is now located at $Stator\ Pitch = 1.4$ has already intersected with this passage vortex. In Fig. 7b, the mechanism of losses in the wake is seen to be different from that of the tip vortex. The streamwise vorticity squeezing of the wake is seen to be correlated with regions of high loss within the wake. Also evident in Figs. 7b and 7c, are the lossy regions of the non-indigenous wakes that originate from the HS stator; these lossy regions are seen to coincide with the short spanwise segments of streamwise vorticity squeezing.

At time $t/T_o=0.12$ the rotor blade now intersects the tip vortex of the second passage. The squeezing in the streamwise normal direction is minimum, compared to that at $t/T_o=0.02$, since the rotor blade obstructs the vortex from being transported downstream. The tip vortex of the first passage is now on the rotor blade pressure side and its stretching in the streamwise direction increases to a maximum. The associated loss coefficient, C_{pt} , is thus minimum. On the otherhand, the tip vortex of the third passage is now closer to the suction side of the rotor blade than at the previous time, $t/T_o=0.02$. Therefore the losses are decreased and C_{pt} within the vortex rises. At time $t/T_o=0.20$ the rotor blade now intersects the tip vortex of the third passage. The vortex squeezing in the streamwise normal direction of the tip vortex in the third passage, due to the blade intersection, and the tip vortex in the first passage, due to its proximity to the rotor blade's suction side, decrease the losses compared to the previous time, $t/T_o=0.12$. However, the tip vortex in the second passage convects downstream, and the attendant vortex elongation in

the streamwise direction increases the losses. The wake can also be identified from the vorticity tilting term involving the radial vorticity as shown in Fig. 10. The flow field of the vorticity tilting term is for time $t/T_o = 0.20$, and can be compared with the flow field at time $t/T_o = 0.02$ that is shown in Fig. 8. No marked time dependent spatial variations of the flow field are evident, however there is a modulation in their intensity this is also confirmed from an animation of the flow field that covered multiple repeating pitches. As is shown schematically in Fig. 10b, the tilting of the radial vorticity associated with the wake, results in the breaking up of the wake into smaller spanwise segments. These smaller spanwise segments are seen as kidney vortex pairs along the span of the wake, which indicate the alternate positive and negative tilting. Although the magnitude of these tilting terms is smaller than the streamwise squeezing of the vorticity, Fig. 8, the enhanced mixing of the small-scale structures contributes to the overall losses of the wake that are dominated by the wake's streamwise squeezing. The enhanced mixing of the small scale structures makes only a small contribution to the overall losses of the wake. This is so since the magnitude of the tilting terms is smaller than the dominant streamwise squeezing of the wake, Fig. 8.

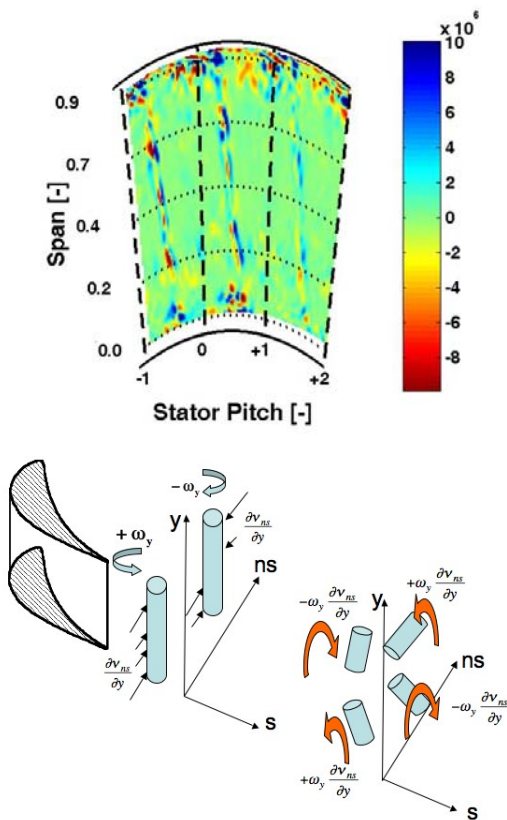


Figure 10: Tilting of wake's radial vorticity at exit of LS stator. (a) Radial vorticity tilting term $\omega_y (\partial v_{ns} / \partial y)$ at downstream measurement plane. Time = $t/T_o = 0.20$ and (b) schematic of wake's breakup mechanism.

Overall, the mechanism of breaking up the continuity of the elongated radial vorticity filaments takes place owing to the tilting. This breakdown process facilitates the downward cascade of the wake's energy from relatively large length scales to smaller scales, which ultimately produces loss. This hypothesis is also supported by the observation that in relatively low aspect ratio HP turbines, wake structures do not survive passage through the downstream blade rows. Rather it is the larger and more dominant passage vortices that entrain the smaller scale vortical structures, thereby concentrating the loss regions within the passage vortices.

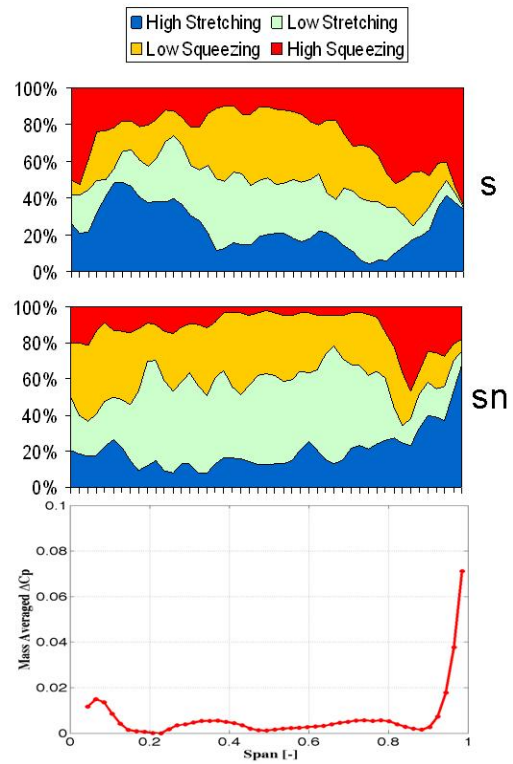


Figure 11: Percentage contribution of low/high stretching/squeezing vorticity terms at exit of LS stator. Most downstream measurement plane at time = $t/T_o = 0.02$. (a) streamwise vorticity stretching term, $\omega_s (\partial v_s / \partial s)$, (b) streamwise normal vorticity stretching term, $\omega_{ns} (\partial v_{ns} / \partial ns)$, and (c) mass averaged relative loss coefficient, ΔC_{pt} .

In Fig. 11, the spanwise distributions of the contribution to loss of the streamwise vorticity stretching and streamwise normal vorticity stretching terms are presented. The range of the stretching/squeezing terms is $\pm 10 \times 10^6 / s^2$. Thus high stretching/squeezing is said to occur when the magnitude of the respective term is greater than $3 \times 10^6 / s^2$, and low stretching/squeezing, when the magnitude is less than $3 \times 10^6 / s^2$. At each spanwise location, the aggregate mass averaged, stagnation pressure loss coefficient is used to normalize the respective contributions. It can be seen that at the outer span, $Span > 0.8$, high streamwise stretching and

high streamwise normal stretching of vorticity are the dominant contributions to loss. The high streamwise normal squeezing at $Span = 0.8$ is associated with tip vortex. The high streamwise squeezing and high streamwise stretching at the tip are associated with leakage flow and skewed boundary layer; these two features are identifiable as the blue regions with a wide circumferential extent that are seen in Figs. 8-11. Within the wake, $0.4 < Span < 0.65$, low streamwise squeezing of vorticity is seen to largely lead to the loss generation. This is not surprising since there is a cascade of wakes, which differs from the case of an isolated wake. In the isolated wake streamwise normal broadening and its attendant mixing would be a dominant loss contributor. However, in the interaction regions of the wake and tip vortex, $0.65 < Span < 0.7$, high streamwise squeezing is seen to lead to significantly to the losses. Wake and secondary flow features that originate in the HS stator are evidenced by the relatively high losses in the spanwise range, $0.2 < Span < 0.4$; as previously described, these non-indigenous features can also be seen in Fig. 7, as the lossy regions whose pitchwise spacing corresponds to that of the HS stator.

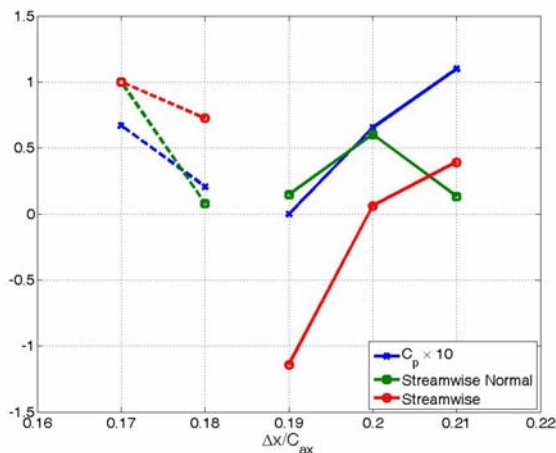


Figure 12: Variation of streamwise stretching, $\omega_s(\partial v_s/\partial s)$, and streamwise normal stretching, $\omega_{ns}(\partial v_{ns}/\partial ns)$, terms in the blade row region between LS stator and rotor. Time = $t/T_o = 0.02$.

The variation of the streamwise and streamwise normal vorticity terms in the gap between the LS stator and second rotor is examined in Fig. 12. The vorticity terms are normalized by the value of the most upstream measurement plane. Also shown in Fig. 12 is pressure coefficient. At the two upstream measurement planes, the measurements were limited to the upper half of the span, whereas at the three downstream planes measurements were made over the full span. The upper half span is dominated by the presence of the tip vortices, which are elongated as they are subsequently convected through the rotor passage. Thus the streamwise stretching vorticity terms are of a relatively large magnitude in these two planes compared to their respective values at the three downstream planes. It is also worthwhile to note that the streamwise stretching decreases as the pressure decreases. Over the downstream measurement planes, the pressure increases as a consequence of the potential field of the

downstream rotor row. Over this region, the streamwise stretching vorticity term closely follows the trend in the pressure distribution. Specifically, this term which indicates streamwise squeezing of vorticity at $\Delta x/C_{ax} = 0.19$ shows that streamwise stretching of vorticity becomes increasingly important in the adverse pressure gradient. On the other hand, the streamwise normal stretching vorticity term shows no strong correlation with the pressure distribution

CONCLUSIONS

Detailed measurements of the unsteady total pressure, velocity and vorticity flowfields at the exit of the second stator in a two-stage, research turbine have been made. The turbine model is representative of the high pressure section of a steam turbine, and the stator rows are of high solidity and low solidity designs respectively. Thus the measurements capture both the unsteady rotor-stator interactions of the second stage as well as the highly three dimensional flowfield that originates upstream. A miniature fast response aerodynamic probe is used to make measurements in five closely spaced planes in the gap between the LS stator and rotor; thus all three components of the vorticity vector can be evaluated without approximation, and all the vorticity stretching and tilting terms of the unsteady vortex transport equation quantified.

The streamwise and streamwise normal vorticity stretching terms are found to be the dominant terms in region of high loss generation. Streamwise elongation and streamwise compression of the vorticity in the tip passage vortices leads to of their loss generation. On the other hand for the wake, streamwise squeezing of vorticity leads to high losses. Although the vorticity tilting terms involving the radial vorticity are less dominant than the stretching terms, they suggest a mechanism of the breaking down of the wake into smaller scale segments that invariably lead, albeit in a small amount, to the wake's losses. Non-indigenous flow features that originate upstream of the second stator are identified, but are observed to be very weak relative to the dominant indigenous passage vortices. These dominant vortical structures entrain and concentrate the lossy regions. In the strive for further improvement in the blading of innovative LS turbines designs these findings provide a turbine designer criteria to achieve enhanced performance.

ACKNOWLEDGMENTS

The authors would like to acknowledge the contributions of Mr. T. Tashima and Mr. T. Sasaki, in the design and development of the turbine test case. The authors also gratefully acknowledge Toshiba Corporation for their support and permission to publish these paper. Thanks are also due to Mr P. Schuepbach for sharing his knowledge in operating the facility and Mr. C. Reshef and Mr. H. Suter for their technical support.

REFERENCES

[1] Binder, R., Romey, A., 1983, "Secondary Flow Effects and Mixing of the Wake Behind a Turbine Stator," ASME J. of Engineering for Gas Turbine and Power, Vol. 105, pp. 40-46

[2] Denton, J., D., 1993, "Loss Mechanisms in Turbomachines," The 1993 IGTI Scholar Lecture, ASME J. of Turbomachinery, Vol. 115, pp. 621-656.

[3] Gregory-Smith, D. G., Graves, C. P., Walsh, J. A., 1987, "Growth of Secondary Losses and Vorticity in an Axial Turbine Cascade," ASME 87-GT-114.

[4] Greitzer, E. M., Tan, C. S., Graf, M. B., 2004, "Internal Flow: Concepts and Applications," Cambridge University Press.

[5] Halstead, D. E., Wisler, D. C., Okiishi, T. H., Walker, G. J., Hodson, H. P., Shin, H.-W., 1997, "Boundary Layer Development in Axial Compressors and Turbines," ASME J. of Turbomachinery, Vol. 119, pp. 248-257.

[6] Langston, L. S., 2001, "Secondary Flows in Axial Turbines-A Review," Heat Transfers in Gas Turbines, Annals of the New York Academy of Sciences, Vol. 934, pp. 11-26.

[7] Lenherr, C., Kalfas, A. I., Abhari, R. S., 2007, "A Flow Adaptive Aerodynamic Probe Concept For Turbomachinery," Meas. Sci. Technol. Vol. 18, pp. 2599-2608.

[8] Miller, R. J., Moss, R. W., Ainsworth, R. W., 2003, "The Development of Turbine Exit Flow in a Swan-Necked Inter-Stage Diffuser," ASME GT2003-38174

[9] Pullan, G., Denton, J., Dunkley, M., 2002, "An Experimental and Computational Study of the Formation of a Streamwise Shed Vortex in a Turbine Stage," ASME GT 2002-30331

[10] Rosic, B., Denton, J. D., Curtis, E. M., Peterson, A. T., 2007, "The Influence of Shroud and Cavity Geometry on

Turbine Performance – An Experimental and Computational Study, Part 2: Exit Cavity Geometry," ASME GT2007 – 27770.

[11] Rusch, D., Pfau, A., Schlienger, J., Kalfas, A. I., Abhari, R. S., 2004, "Deterministic Unsteady Vorticity Field in a Driven Axisymmetric Cavity Flow," J. of Computational and Applied Mechanics, Vol. 5., pp. 235-247

[12] Schlienger, J., Kalfas, A. I., Abhari, R. S., 2004, "Vortex-Wake-Blade Interaction in a Shrouded Axial Turbine," ASME GT-2004-53915

[13] Schlienger, J., Pfau, A., Kalfas, A. I., Abhari, R. S., 2003, "Effects of Labyrinth Seal Variation on Multistage Axial Turbine Flow," ASME GT2003-38270

[14] Sharma, O. P., Butler, T. L., Joslyn, H. D., Dring, R. P., 1985, "Three-Dimensional Unsteady Flow in an Axial Flow Turbine," AIAA J. of Propulsion and Power, Vol. 1, pp. 29-38.

[15] Sieverding, C. H., 1985, "Recent Progress in the Understanding of Basic Aspects of Secondary Flows in Turbine Blade Passages," ASME J. of Turbomachinery, Vol. 107, pp. 248-257.

[16] Tashima, T., Sasaki, T., Kalfas, A. I., Abhari, R. S., 2007, "Blade Loading Influence on Unsteady Flow Interactions In Axial Steam Turbines," ASME GT2007-27452

[17] Treiber, M., Abhari R. S., Sell, M., 2002, "Flow Physics and Vortex Evolution in Annular Turbine," ASME GT-2002-30540.

[18] Zaccaria, M., Lakshminarayana, B., 1995, "Investigation of three dimensional Flowfield at the Exit of a Turbine Nozzle," AIAA J. of Propulsion and Power, Vol. 11, pp. 55-63